International Journal of Impact Engineering 42 (2012) 80–88

Contents lists available at SciVerse ScienceDirect

International Journal of Impact Engineering

journal homepage: www.elsevier.com/locate/ijimpeng

Crushing and crashing of tubes with implicit time integration

Zafer Kazancı [a,b,*], Klaus-Jürgen Bathe [b]

[a] Turkish Air Force Academy, Aerospace Engineering Department, 34149 Yeşilyurt, Istanbul, Turkey
[b] Massachusetts Institute of Technology, Department of Mechanical Engineering, 77 Massachusetts Avenue, MA 02139, United States

ARTICLE INFO

Article history:
Received 10 August 2011
Received in revised form
13 October 2011
Accepted 16 October 2011
Available online 25 October 2011

Keywords:
Dynamic axial crushing
Implicit time integration
Bathe method
3D-shell element
Crash tube

ABSTRACT

The axial crushing and crashing of thin-walled high-strength steel tubes is performed using 3D-shell finite elements and an implicit time integration scheme. The calculated results are compared with published experimental data and results obtained using explicit time integration. The objective is to show that, while for such analyses generally explicit time integration is used, with the current state of the art also an implicit time integration solution should be considered, and such solution approach can provide an effective alternative for a simulation.

1. Introduction

The crush and crash worthiness of a vehicle is today of great importance. Strict standards need to be adhered to in the industry, in particular to protect human life. In the aim for better performance, the design of vehicles has also evolved to improve protection capabilities. In order to decrease design times and ensure safe design standards regarding the crush and crash worthiness of vehicles, and their components, virtual tests are usually performed in numerical simulations. The virtual crush and crash test data are used throughout the entire development of a new design. These numerical simulations produce results without building a physical model, and can be performed relatively quickly and inexpensively. This permits optimization of the design before an actual prototype of the vehicle has to be built.

The most important phenomenon in a crush or crash situation is to absorb the kinetic energy. Crash tubes are designed for that purpose and are used in many practical situations. They have the ability to absorb and convert large amounts of kinetic energy into plastic strain energy under severe loading conditions. Therefore, there has been continued interest on the axial crushing and crashing behavior of tubes [1–10]. Wierzbicki and Abramowicz [1] developed a theory which describes the crushing behavior of a class of thin-walled structures. Jones [2–4] reviewed the dynamic plastic behavior of structures in conditions of impacts. Alghamdi [5] summarized the common shapes of collapsible energy absorbers and their most common deformation shapes. Jones [6] discussed the dynamic inelastic buckling of structural members. Schneider and Jones [7] conducted some experimental studies on quasi-static crushing and dynamic axial collapse of thin-walled high-strength steel structural sections. Olabi et al. [8] reviewed metallic tube type energy absorbers in which predominantly mild steel and/or aluminum materials are used. Yuen and Nurick [9] reviewed the response of tubular structures with geometrical/material imperfections subjected to axial loading. Karagiozova and Alves [10] summarized the dynamic inelastic stability and postbuckling behavior of various basic structural members.

For years now, finite element methods [11] have been used for the nonlinear dynamic analyses of structures, like cars, airplanes, ships, submarines, bridges, to name a few. Two kinds of time stepping algorithms are available for these analyses – explicit and implicit techniques. If the solution for time $t + \Delta t$ is based on using the equilibrium conditions at time t, the integration procedure is called an explicit integration method. Such integration schemes are conditionally stable, that is, require a time step size small enough for stability, but do not require a factorization of an (effective) stiffness matrix in the step-by-step solution, that is, the integration is simply marched forward without any iteration. On the other

* Corresponding author. Turkish Air Force Academy, Aerospace Engineering Department, 34149 Yeşilyurt, Istanbul, Turkey. Tel.: +90 212 6632490x4340; fax: +90 212 6628554.
E-mail address: z.kazanci@hho.edu.tr (Z. Kazancı).

0734-743X/$ – see front matter © 2011 Elsevier Ltd. All rights reserved.
doi:10.1016/j.ijimpeng.2011.10.003

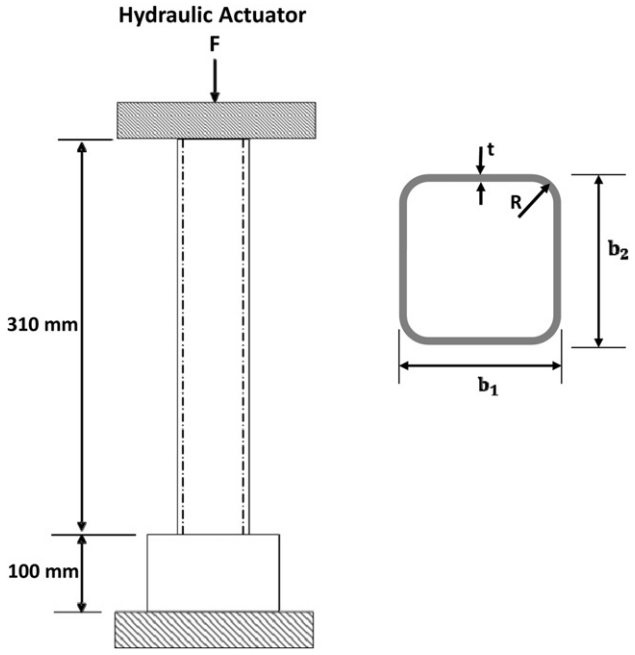

Fig. 1. Schematic of geometry and experimental set-up for quasi-static case.

hand, if the method uses the equilibrium conditions at time $t + \Delta t$, to calculate the solution at time $t + \Delta t$, the technique is called an implicit integration method [11,12]. These methods can be designed to be unconditionally stable in linear analyses but an effective stiffness matrix is employed. In nonlinear analyses, tangent stiffness matrices are used and equilibrium iterations are performed to obtain the solution at time $t + \Delta t$. It is clear that, therefore, the numerical effort per time step solution is much larger in an implicit integration than in an explicit integration – and this assumes that, indeed, an implicit time integration simulation can actually be performed, that is, iteration convergence is reached in each time step. Also, while a method may be unconditionally stable in linear analysis, the method may not perform sufficiently well in nonlinear solutions – in fact, even the widely-used trapezoidal rule does not perform well in large deformation and long-time duration analyses [13].

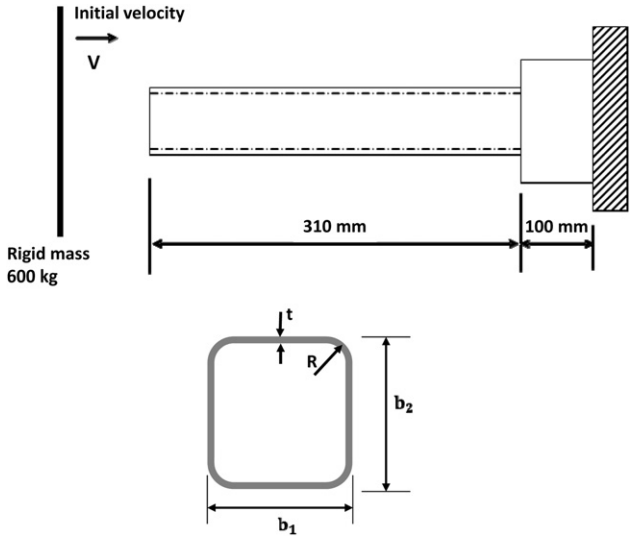

Fig. 2. Schematic of geometry and experimental set-up for dynamic cases.

Table 1
Quasi-static case, crush tube geometrical parameters (mm).

	b_1	b_2	t	R
Ref. [23]	60.6	60.6	1.20	3
Present study	59.3	58.0	1.18	3
qs 01 (experiment)	59.3	58.0	1.18	3

In today's engineering practice, generally, for crush and crash simulations explicit time integration schemes are used. If a small time step is indeed required to trace out the dynamic response, and the maximum response is reached in a short time interval, an explicit time integration is clearly most effective. However, in some analyses, a time step size orders of magnitude larger would trace out the dynamic response adequately and the response needs to be calculated over a long-time span. In this case, implicit integration would ideally be used. Nevertheless, even in such cases, explicit integration is widely employed because convergence in the iterations of an implicit integration is not achieved. Indeed, it is for this reason that rather nonphysical schemes are used in explicit integration, like 'artificial mass scaling' allowing a larger time step size, merely to be able to obtain a solution with a reasonable solution effort. In these cases, an implicit time integration solution could be much more effective and reliable – assuming that the solution is actually achieved in a stable and accurate manner with a large time step size and good iteration convergence in each step.

Simulations where implicit time integration may be of value are clearly found in the crush and crash analyses of motor cars, but also when modeling collisions of trains and ships.

Considering relatively recent studies in which explicit integration was used, Jensen et al. [14] conducted a parametric study of the transition between progressive and global buckling of axially loaded aluminum extrusions. Rossi et al. [15] studied the deformation characteristics of aluminum alloy extruded polygonal section tubes subjected to dynamic axial impacts. Aktay et al. [16] investigated the quasi-static axial crushing of empty and foam-filled aluminum tubes and discussed their energy absorption characteristics. Zhang and Huh [17] studied the energy absorption characteristics of longitudinally grooved square tubes. Fyllingen et al. [18] investigated the influence of the element type and formulation for modeling aluminum profiles subjected to axial loading. Kaya and Öztürk [19] studied the effects of the cross-sectional shapes of profiles on the crush behavior. Guler et al. [20] examined the effects of wall thickness and cross-sectional geometry on the performance characteristics of the energy absorbers. Nia and Hamadani [21] investigated the deformation modes and energy absorption capacities of thin-walled tubes with various cross-sectional geometries and compared the

Table 2
Dynamic case, crash tube geometrical parameters (mm).

	b_1	b_2	t	R
(a) V = 5 m/s				
Ref. [23]	60.6	60.6	1.20	3
Present study	59.7	56.8	1.17	3
ds02 (experiment)	59.7	56.8	1.17	3
(b) V = 10 m/s				
Ref. [23]	60.6	60.6	1.20	3
Present study	59.1	57.2	1.18	3
ds04 (experiment)	59.1	57.2	1.18	3
(c) V = 15 m/s				
Ref. [23]	60.6	60.6	1.20	3
Present study	60.0	57.8	1.17	3
ds06 (experiment)	60.0	57.8	1.17	3

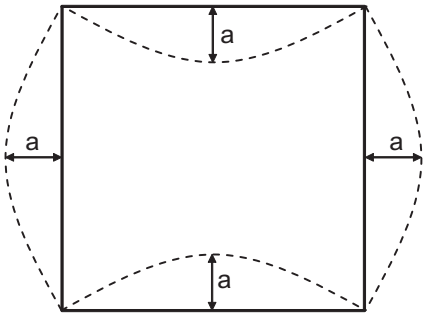

Fig. 3. Geometrical imperfections (amplitude a = 0.05 mm).

experimentally and numerically obtained data. Toksoy and Güden [22] optimized the energy absorption of partially foam-filled crash boxes. Furthermore, Tarigopula et al. [23] performed axial quasi-static crush and dynamic crash tests of thin-walled sections made of high-strength steels.

There have also been a few studies using implicit time integration. Mamalis et al. [24] simulated the crush behavior of cylindrical composite tubes under static and dynamic axial compression using an implicit finite element code. Koganti and Caliskan [25] analyzed the crash behavior of a circular tube, and the results showed that the tube thickness and yield strength variations significantly affect the crush behavior. Also, hybrid explicit/implicit time marching schemes were presented, see Noels et al. [26] and Lo et al. [27], and were used to sometimes reduce the computational time significantly.

However, altogether, still, relatively little experience is available using implicit time integration schemes for crush and crash simulations. Our objective in this paper is to give our experiences in that field. We focus on the use of an implicit time integration method and demonstrate its use in crush and crash analyses. Although the use of explicit time integration has been refined over many years of applications, we believe that an implicit time integration solution, if stable, accurate and efficient, can be very attractive for many crush and crash applications – at least as an alternative solution approach. For the time integration, we use the method published in refs. [13,28]. This implicit time integration scheme was shown to be

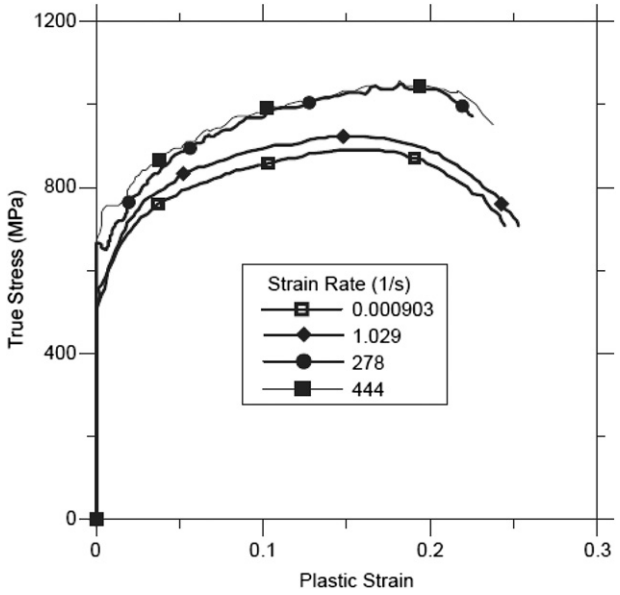

Fig. 4. True-stress versus true-plastic strain curves at different strain rates for DP800 high-strength steel [23].

Table 3
Material properties for DP800 high-strength steel [23].

σ_0 (N/mm^2)	Q_1 (N/mm^2)	C_1	Q_2(N/mm^2)	C_2	$\dot{\varepsilon}_0$ (1/s)	q
495	200	76	233	10	0.001	0.0116

effective, without the use of artificial factors, in cases where the traditional trapezoidal rule fails to give a solution, namely in transient response analyses of structures when large deformations and long-time durations are considered. Additionally, we use the 3D-shell element available in ADINA [29], which is effective in very large deformation and large elastic–plastic strain solutions.

2. Problem considered

We perform the crush and crash analyses of the tubes considered in ref. [23]. In this reference, experimental data and results obtained using explicit time integration are given, with which we can compare our computed solutions. In each case, a thin-walled tube of square cross-section and high-strength steel is considered. Figs. 1 and 2 show schematically the geometry, loading and boundary conditions of the tubes for the quasi-static crush and the dynamic crash cases, respectively. The slightly different cross-sectional dimensions for the different test cases are given in Tables 1 and 2. Here, b_1 and b_2 are the outer dimensions in the x- and y-directions, t is the thickness, and R is the corner radius. As can be seen from the tables, we used the experimentally measured geometrical values in our solutions (except for the results in Fig. 12), while Tarigopula et al. [23] used average dimensions for their numerical simulations (these are listed in the tables). As in ref. [23], we introduced a geometrical imperfection described by a half sine wave across each of the four sides, with constant imperfection values in the longitudinal direction from the top to the start of the

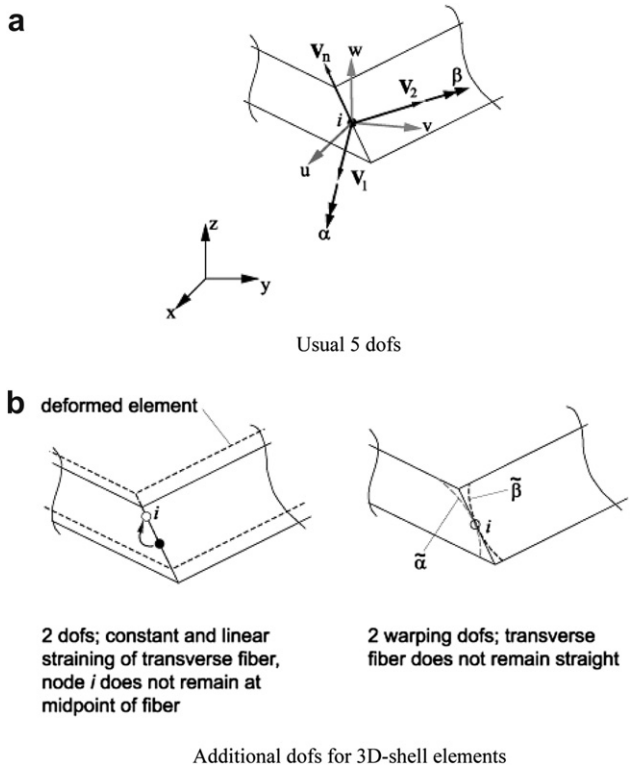

Fig. 5. 3D-shell element, degrees of freedom.

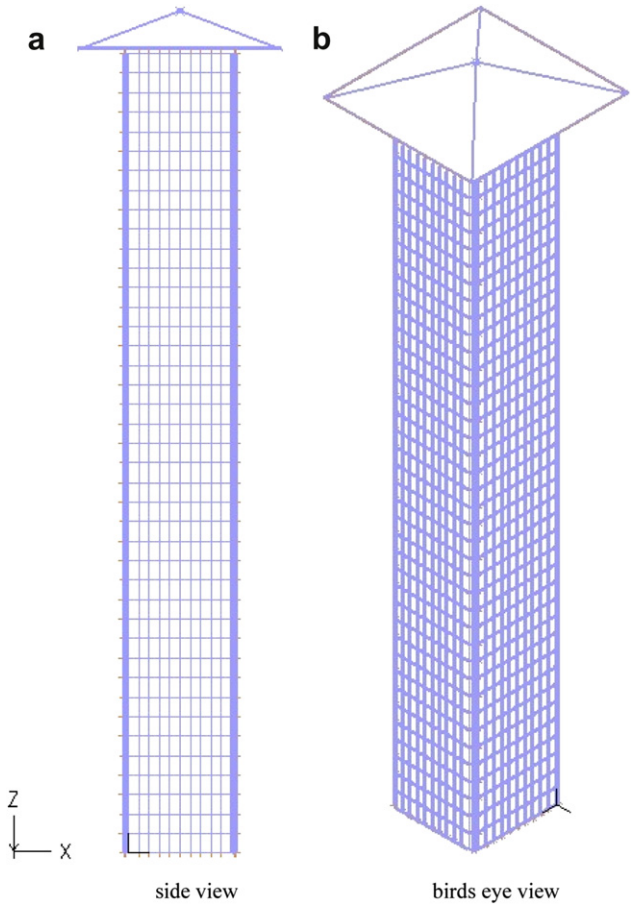

Fig. 6. Finite element model (mesh density 41 × 10 per side).

constrained bottom part. This imperfection was introduced with the in-ward and the out-ward patterns on opposing sides in order to match with a regular folding mode, see Fig. 3.

The total length of the tubes is 410 mm; however, the lower 100 mm are constrained. To characterize the material behavior, we use the true-stress versus true-plastic strain curves given by

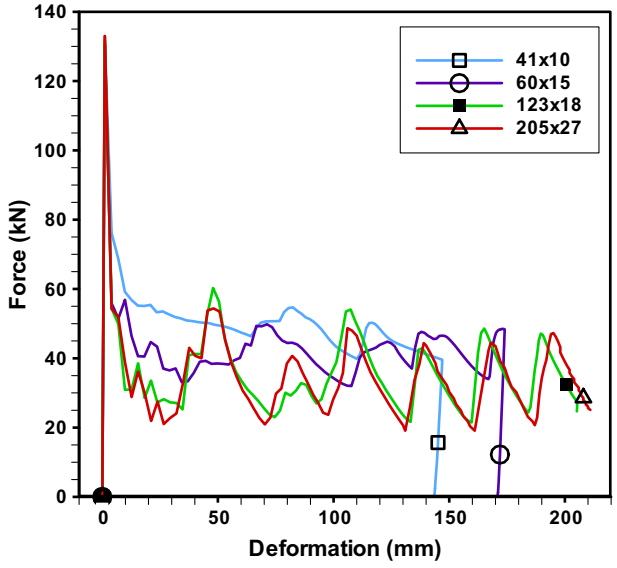

Fig. 7. Convergence study for suitable mesh density (V = 5m/s).

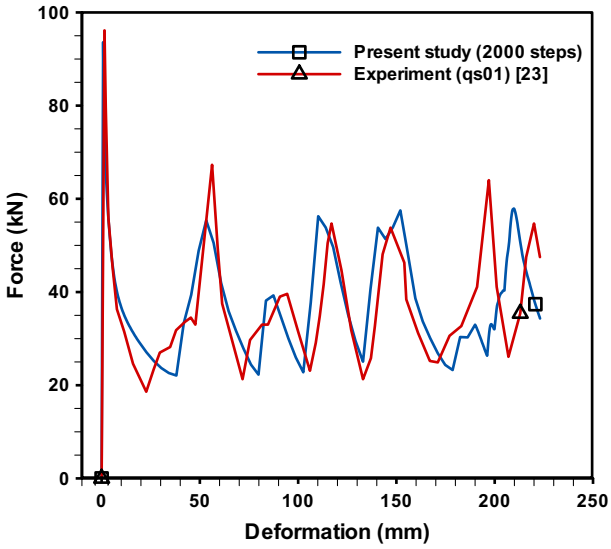

Fig. 8. Comparison for the quasi-static case (2000 steps).

Tarigopula et al. [23] (see Fig. 4). The authors gave an empirical constitutive equation for the effective stress at yield, $\bar{\sigma}$, as a function of the effective plastic strain, $\bar{\varepsilon}$, representing the data in Fig. 4 as

$$\bar{\sigma}(\bar{\varepsilon}) = \left(\sigma_0 + \sum_{i=1}^{2} Q_i(1-\exp(-C_i\bar{\varepsilon}))\right)\left(1+\frac{\dot{\bar{\varepsilon}}}{\dot{\varepsilon}_0}\right)^q \quad (1)$$

where σ_0 is the initial yield stress, and Q_i and C_i are strain-hardening coefficients, q is a material constant and $\dot{\varepsilon}_0$ is a user-defined reference strain rate. The material constants are given in ref. [23] and are also listed in Table 3. The density of the material is 7850 kg/m^3, the modulus of elasticity is 195 GPa, and Poisson's ratio is 0.33. As seen in Fig. 4, the increase in the yield stress during material flow is approximately 15% when increasing the strain rate from about 10^{-3} to 500/s.

For the quasi-static case, the tube was crushed in an Instron 250kN testing machine. For the dynamic crash case, the tubes were impacted by a rigid weight of total mass 600 kg with the initial velocities 5, 10 and 15 m/s.

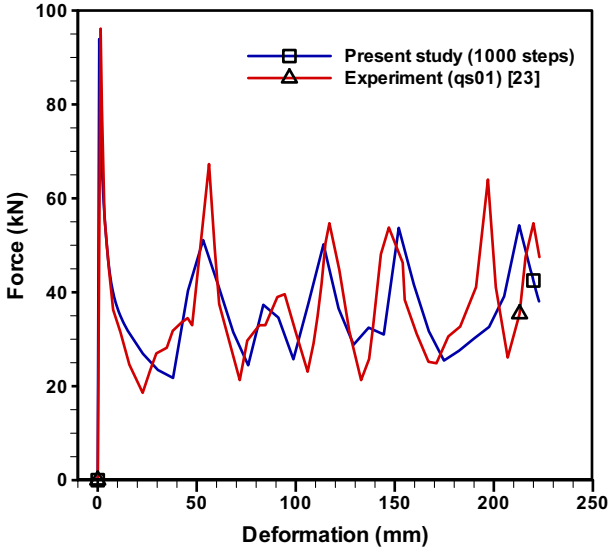

Fig. 9. Comparison for the quasi-static case (1000 steps).

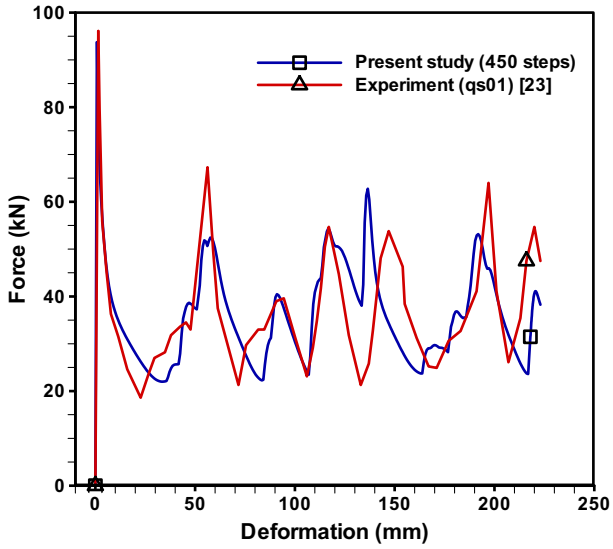

Fig. 10. Comparison for the quasi-static case (450 steps).

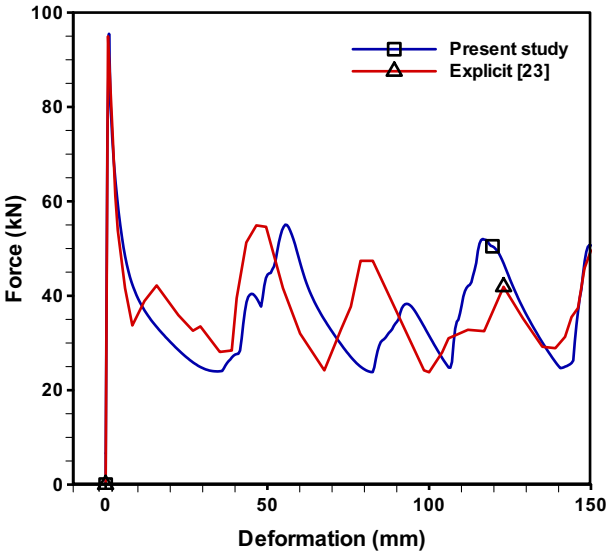

Fig. 12. Force-displacement curves for the implicit and explicit solutions, in both cases using the geometric data of ref. [23] given in Table 1.

3. Solution methods – briefly

In each response solution, we solved the governing dynamic equilibrium equations

$$\mathbf{M}\ddot{\mathbf{U}} + \mathbf{F}\left(\mathbf{U},\ time\right) = \mathbf{R}\left(time\right) \text{ (plus initial conditions)} \qquad (2)$$

where **M** is the mass matrix, **U** is the vector of nodal point displacements and rotations, **F** denotes the vector of nodal point forces corresponding to the internal element stresses, **R** is the vector of externally applied nodal point loads, and an overdot denotes time derivative. Note that all time-dependent quantities, like the plastic effects, are understood to vary in Eq. (2) [11].

For the implicit time integration we used the method proposed by Bathe [13]. Here the time increment Δt is divided into two equal sub-steps. In the first sub-step, the trapezoidal rule is used and in the second sub-step the 3-point Euler backward method is employed. While the trapezoidal rule and the Euler method have, of course, been used for many years (see for example ref. [30]), the two sub-steps composite scheme was first time shown in refs.

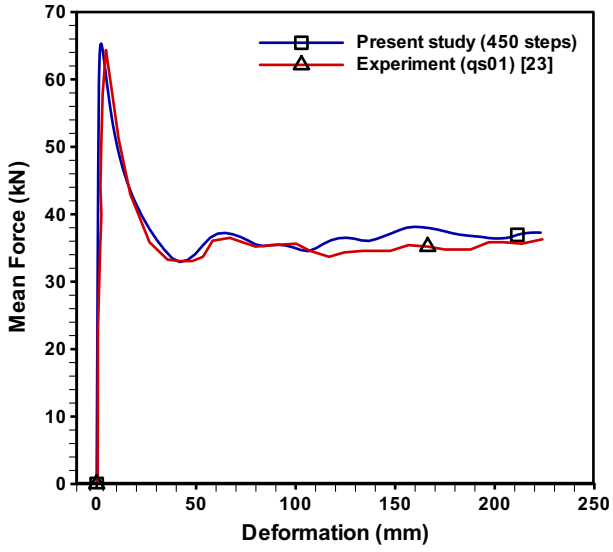

Fig. 11. Mean crushing force versus displacement for the quasi-static case.

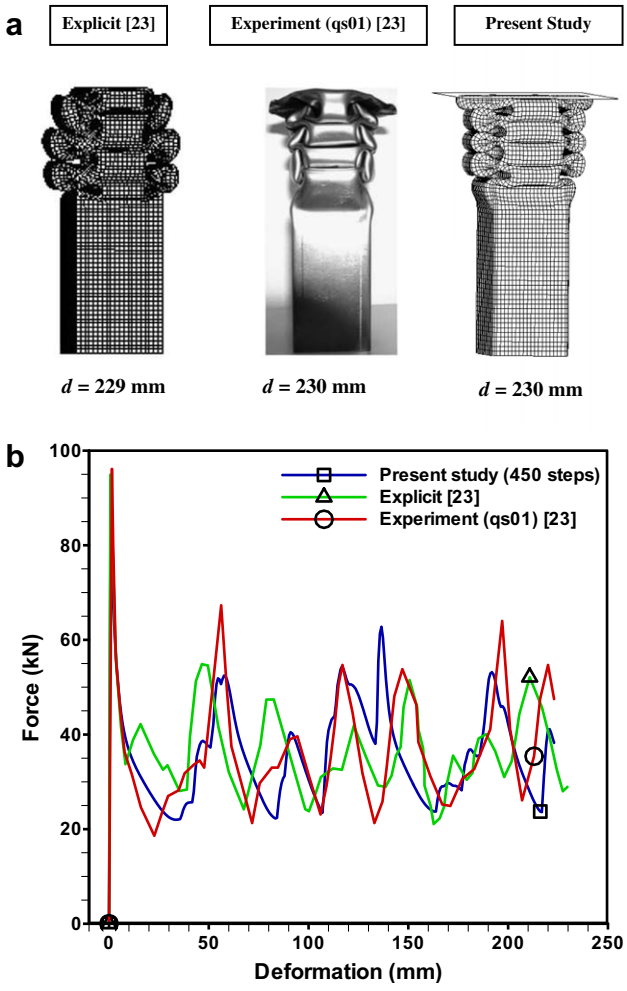

Fig. 13. Comparison of computed results versus test results: (a) final deformations and (b) force-displacement curves.

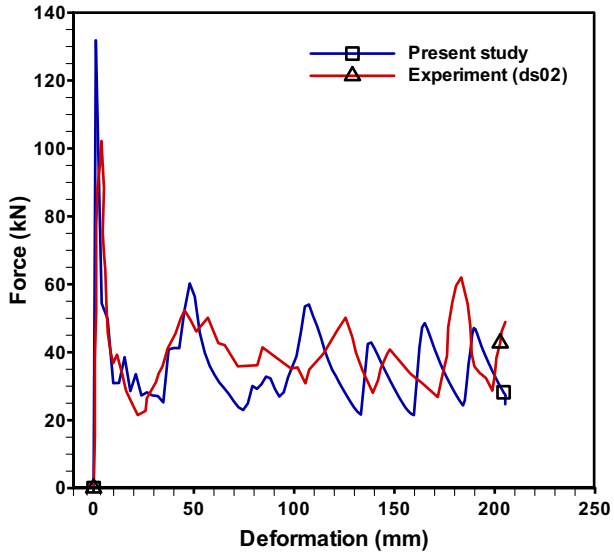

Fig. 14. Comparison of force-displacement curves (V = 5 m/s).

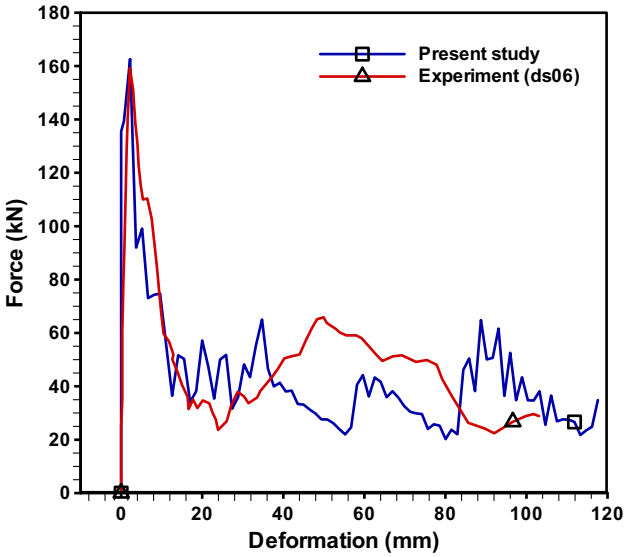

Fig. 16. Comparison of force-displacement curves (V = 15 m/s).

[13,28] to be effective in the solution of nonlinear structural dynamics, and the benefits were studied and summarized.

The tube was modeled using the 4-node 3D-shell element available in ADINA [29]. This element is appropriate to model very large deformations with large plastic strains using the Updated Lagrangian Hencky formulation [11,31]. This plasticity formulation is a 'total strain formulation' which is preferable to a Jaumann rate type formulation [11,32]. An important point is that this 3D-shell element can be employed in explicit and implicit dynamic solutions and in static analyses, since no reduced integration with hourglass control is used, and there are no artificial stability factors in the formulation. These 3D-shell elements build upon the conventional MITC elements [11,33–35], with 5 or 6 degrees of freedom at each node, but have these additional features, when invoked by degrees of freedom:

- Two additional through-the-thickness strain degrees of freedom to allow large strains through the element thickness.
- Warping degrees of freedom to allow the transverse fibers to warp, that is, these originally straight fibers, when allowed, do not remain straight during the deformations.

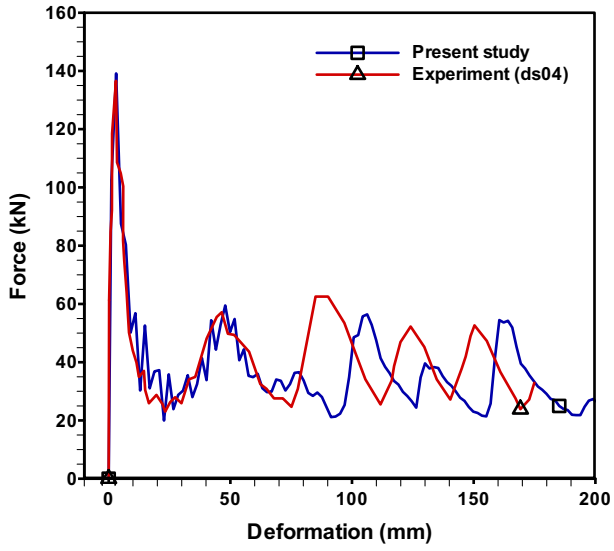

Fig. 15. Comparison of force-displacement curves (V = 10 m/s).

The two through-the-thickness degrees of freedom allow the element to model a constant and a linear strain distribution through the shell thickness. The two extra warping degrees of freedom (3 warping degrees of freedom when there are 3 usual rotational degrees of freedom) allow the transverse fibers to warp in a quadratic displacement, see Fig. 5. Thus, while all degrees of freedom are defined at the shell mid-surface nodes, from a displacement interpolation point of view, the element can be thought of as a higher-order 3D solid element when the additional degrees of freedom are invoked. In all our solutions given below, we used this 3D-shell element with 5 point Gauss numerical integration through the thickness. The contact conditions are imposed using the algorithm described in ref. [36].

4. Numerical simulations

In this section, we give the results of our numerical simulations using ADINA for the quasi-static crushing and the dynamic crashing of the thin-walled high-strength steel section tubes described above, and compare the results to those published in ref. [23]. The numerical results in that reference were obtained using LS-DYNA.

4.1. The finite element model

Fig. 6 shows a rather coarse mesh using the 4-node 3D-shell element with 5 degrees of freedom at each node. To identify an appropriate mesh, we carried out several simulations by increasing the mesh density. The results are shown in Fig. 7, where the numbers given refer to the mesh used for one side of the tube. The 41x10 and 60x15 meshes are clearly too coarse but the 123x18 mesh is sufficiently fine resulting into a total of 10,332 shell

Table 4
Comparison of final mean crush and crash forces, P_m (kN).

	Experimental [23]	Analytical [23]	Explicit [23]	Present study
Quasi-static (qs01)	36.2	47.9	36.9	37.1
V = 5 m/s (ds02)	39.2	50.6	37.8	36.4
V = 10 m/s (ds04)	42.5	51.3	44.9	40.1
V = 15 m/s (ds06)	48.5	51.8	49.8	43.2

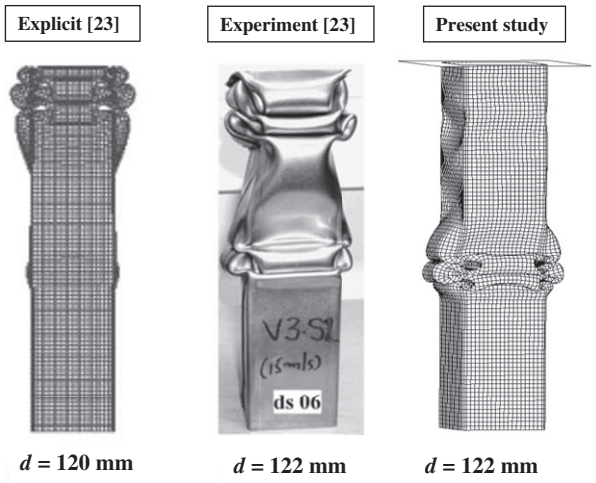

Fig. 17. Comparison of final deformations (V = 15 m/s).

elements. In the mesh, three elements are placed along the arcs in the corners. Considering the bottom part of 100 mm, to model the experimental set-up as in ref. [23], we fixed all shell degrees of freedom except for the translations into the longitudinal direction. Also, the rotational degrees of freedom were fixed at the free end of the tube. A rigid surface-block was linked rigidly to a single master node. In the crush case, the displacement was imposed at that node. In the crash cases, the block represented the rigid mass and the initial velocity was given to the master node. The contact between the rigid surface and the tubes was modeled with a friction coefficient of 0.3, while for self-contact of the tube frictional effects were neglected. For all solutions, we used the Bathe implicit time integration method briefly described already above.

4.2. Quasi-static crush case

For the quasi-static crush case, we used the data of the experiment qs01 from ref. [23]. In that study, the velocity was ramped artificially in the explicit solutions in order to reduce the number of time steps to be used. In our solution, we of course did not use any artificial technique. We applied the total end displacement of 230 mm in 2000, 1000 and 450 equal time steps, each time

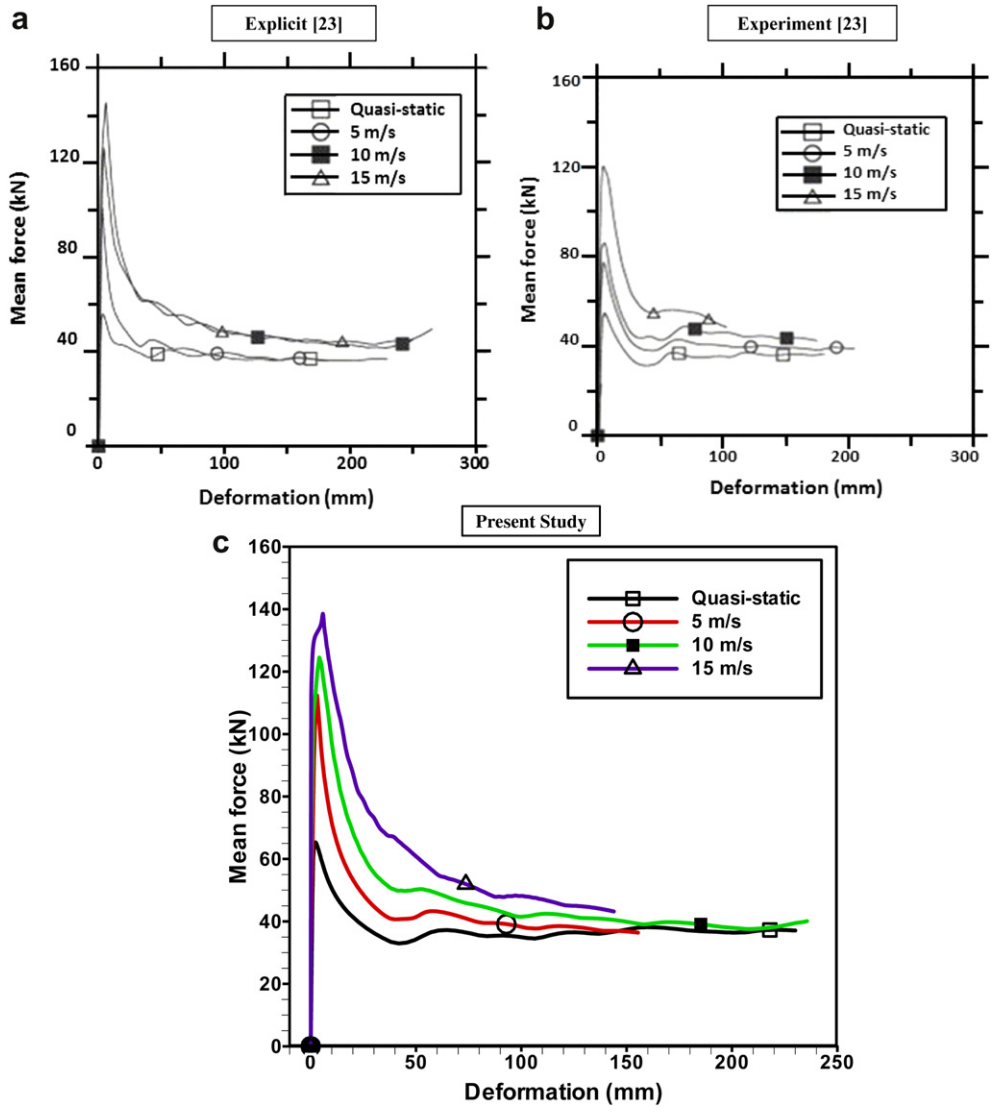

Fig. 18. Comparison of the predicted and measured mean force versus displacement curves.

spanning over the duration of 1000 s, which corresponds to quasi-static conditions and the experimental set-up in ref. [23]. The results are compared with the experimental data in Figs. 8–10, respectively. Our 450 time step solution took about 2 1/2 h to run using a desktop computer equipped with an Intel i7 X990 CPU at 3.47 GHz.

In Fig. 11, we refer to the mean crushing force P_m at the deformation d defined as

$$P_m = \frac{1}{d}\int_0^d P(\delta)\mathrm{d}\delta \tag{3}$$

where $P(\delta)$ is the instantaneous crushing load corresponding to the instantaneous shortening δ. The instantaneous crushing load is given in Figs. 8–10. A comparison of the mean crushing force versus deformation of the experimental data and our 450 time step solution is shown in Fig. 11. The results agree very well.

Fig. 12 shows a comparison of the published explicit quasi-static results and our 450 steps implicit solution when we use the geometric data of ref. [23] (note that our results in Figs. 10 and 12 are different because different geometric data were used, see Table 1). There is reasonable agreement between the implicit and explicit time integration results.

Fig. 13 shows the axial deformation patterns and the load-displacement curves. The deformation patterns correspond to the maximum axial deformations. The numerical results are in reasonable agreement with the experimental findings, but the deformations of our shell model indicate in certain areas a too stiff behavior. By the assumptions of the shell theory [35], the model is clearly too stiff along the longitudinal corners.

4.3. Dynamic crash cases

In this study, we solved for the response corresponding to the three experiments ds02, ds04 and ds06 of ref. [23], see Table 2a–c. The load was applied to the free end by the 600 kg mass with initial velocities 5 m/s, 10 m/s and 15 m/s, respectively, and the time step we used in each case was $\Delta t = 10^{-5}$ s. Figs. 14–16 show our solutions and the experimental results for the three cases. Considering Fig. 14, there is a considerable difference between the experimentally measured peak force and the computed result. However, while the calculated *peak* force is higher, the calculated *mean* force is actually lower, see Table 4. On the other hand, for the experiments ds04 and ds06, our computed results agree very well with the experimentally measured peak force values (see Figs. 15 and 16).

Fig. 17 shows some axial deformation behavior of the crash tube subjected to the initial block velocity of 15 m/s. The deformations obtained from the explicit and implicit solutions are shown and compared with the experimental findings. Our results agree with the experimental deformation patterns in the middle of the tube, but our solution did not predict the collapse of the section at the top. In the explicit solution, the collapse at the top has been predicted but the deformations near the middle of the tube are not like seen in the experiment.

Fig. 18 shows a comparison of the predicted and the measured mean force values versus displacement curves. The experimental results are lower in the initial response, except for the quasi-static case, when compared to the computed results. Comparisons of the final mean crush forces considering the experimental results, the numerical solutions, and results obtained using an analytical formula (these results are taken from ref. [23]) are also given in Table 4. The agreement between the predicted mean force levels and the experimentally measured values is reasonable, but our results are generally not quite as close to the experimental data as the explicit solutions reported in ref. [23], with the discrepancy largest for experiment ds06.

5. Concluding remarks

The objective of this paper is to show that an implicit time integration solution can be a reliable alternative to an explicit solution for some crush and crash problems. We used the Bathe time integration method and the 3D-shell element with contact conditions, available in ADINA, to solve some tube crush and crash problems. The computed results were compared with published experimental data and published solutions obtained using explicit time integration. Overall good agreement between the computed solutions and the experimental results was seen; however, only a single structural geometry was considered, and further studies using other geometries and physical conditions would be valuable. For example, the material conditions shown in Fig. 4 correspond to only mild softening; conditions of stronger softening, and some fracture as well, can in principle be included but should be studied. Also, columns of large width-to-thickness ratios are notoriously sensitive to initial imperfections [37] and hence might need a special approach included in explicit and implicit time integrations.

While explicit time integration is now widely used for crush and crash analyses, it is well known that the use of such integration scheme to solve certain problems, notably low speed dynamic or almost static problems, can lead to difficulties. In such cases, an implicit time integration solution may well be more suitable – or might at least provide a valuable alternative in the solution approach.

References

[1] Wierzbicki T, Abramowicz W. On the crushing mechanics of thin-walled structures. Journal of Applied Mechanics 1983;50(4):727–34.
[2] Jones N. Recent studies on the dynamic plastic behavior of structures. Applied Mechanics Review 1989;42(4):95–115.
[3] Jones N. Recent studies on the dynamic plastic behavior of structures-an update. Applied Mechanics Review 1996;49(10):112–7.
[4] Jones N. Structural impact. Cambridge, UK: Cambridge University Press; 1997.
[5] Alghamdi AAA. Collapsible impact energy absorbers: an overview. Thin-Walled Structures 2001;39(2):189–213.
[6] Jones N. Several phenomena in structural impact and structural crashworthiness. European Journal of Mechanics A/Solids 2003;22(5):693–707.
[7] Schneider F, Jones N. Impact of thin-walled high-strength steel structural sections. Proceedings of the Institution of Mechanical Engineers, Part D. Journal of Automobile Engineering 2004;218(2):131–58.
[8] Olabi AG, Morris E, Hashmi MSJ. Metallic tube type energy absorbers: a synopsis. Thin-Walled Structures 2007;45:706–26.
[9] Yuen SCK, Nurick GN. The energy-absorbing characteristics of tubular structures with geometric and material modifications: an overview. Applied Mechanics Reviews 2008;61(2):020802.
[10] Karagiozova D, Alves M. Dynamic elastic-plastic buckling of structural elements: a review. Applied Mechanics Reviews 2008;61(4):040803.
[11] Bathe KJ. Finite element procedures. Prentice Hall, 1996 (published by KJ Bathe, 2006).
[12] Kojic M, Bathe KJ. Inelastic analysis of solids and structures. Berlin, Germany: Springer; 2005.
[13] Bathe KJ. Conserving energy and momentum in nonlinear dynamics: a simple implicit time integration scheme. Computers & Structures 2007;85:437–45.
[14] Jensen Ø, Hopperstad OS, Langseth M. Transition from progressive to global buckling of aluminium extrusions – a numerical study. International Journal of Crashworthiness 2005;10(6):609–20.
[15] Rossi A, Fawaz Z, Behdinan K. Numerical simulation of the axial collapse of thin-walled polygonal section tubes. Thin-Walled Structures 2005;43:1646–61.
[16] Aktay L, Toksoy AK, Güden M. Quasi-static axial crushing of extruded polystyrene foam-filled thin-walled aluminum tubes: experimental and numerical analysis. Materials & Design 2006;27:556–65.
[17] Zhang X, Huh H. Energy absorption of longitudinally grooved square tubes under axial compression. Thin-Walled Structures 2009;47:1469–77.
[18] Fyllingen O, Hopperstad OS, Hanssen AG, Langseth M. Modelling of tubes subjected to axial crushing. Thin-Walled Structures 2010;48:134–42.
[19] Kaya N, Öztürk F. Multi-objective crashworthiness design optimisation of thin-walled tubes. International Journal of Vehicle Design 2010;52:54–63.

[20] Guler MA, Cerit ME, Bayram B, Gerceker B, Karakaya E. The effect of geometrical parameters on the energy absorption characteristics of thin-walled structures under axial impact loading. International Journal of Crashworthiness 2010;15(4):377–90.
[21] Nia AA, Hamedani JH. Comparative analysis of energy absorption and deformations of thin walled tubes with various section geometries. Thin-Walled Structures 2010;48(12):946–54.
[22] Toksoy AK, Güden M. The optimisation of the energy absorption of partially Al foam-filled commercial 1050H14 and 6061T4 Al crash boxes. International Journal of Crashworthiness 2011;16(1):97–109.
[23] Tarigopula V, Langseth M, Hopperstad OS, Clausen AH. Axial crashing of thin-walled high-strength steel sections. International Journal of Impact Engineering 2006;32:847–82.
[24] Mamalis AG, Manolakos DE, Ioannidis MB, Kostazos PK, Chirwa EC. Static and dynamic axial collapse of fibreglass composite thin-walled tubes: finite element modeling of the crush zone. Environmental Modeling and Assessment 2003;8(3):247–54.
[25] Koganti RP, Caliskan AG. Stochastic applications in crashworthiness. In: Proceedings of 2001 ASME International Mechanical Engineering Congress and Exposition. NY, USA: New York; November 11–16, 2001. p. 89–96.
[26] Noels L, Stainier L, Ponthot JP. Combined implicit/explicit algorithms for crashworthiness analysis. International Journal of Impact Engineering 2004; 30:1161–77.
[27] Lo C, Hinnerichs T, Hales J. Assessment of efficiency for a hybrid explicit/implicit code simulation of a multiple impact crash scenario. In: Proceedings of 2005 ASME International Mechanical Engineering Congress and Exposition. Florida, USA: Orlando; November 5-11, 2005. p. 381–6.
[28] Bathe KJ, Baig MMI. On a composite implicit time integration procedure for nonlinear dynamics. Computers & Structures 2005;83:2513–34.
[29] ADINA Theory and Modeling Guide, ADINA R & D, Inc., Watertown, MA, USA, 2010.
[30] Collatz L. The numerical treatment of differential equations. 3rd ed. New York: Springer-Verlag; 1966.
[31] Montans FJ, Bathe KJ. Computational issues in large strain elasto-plasticity: an algorithm for mixed hardening and plastic spin. International Journal for Numerical Methods in Engineering 2005;63:159–96.
[32] Kojic M, Bathe KJ. Studies of finite element procedures—stress solution of a closed elastic strain path with stretching and shearing using the updated Lagrangian Jaumann formulation. Computers & Structures 1987;26:175–9.
[33] Bathe KJ, Lee PS. Measuring the convergence behavior of shell analysis schemes. Computers & Structures 2011;89:285–301.
[34] Kim DN, Bathe KJ. A 4-node 3D-shell element to model shell surface tractions and incompressible behavior. Computers & Structures 2008;86:2027–41.
[35] Chapelle D, Bathe KJ. The finite element analysis of shells – fundamentals. 2nd ed. Berlin, Germany: Springer; 2003. 2011.
[36] Bathe KJ, Bouzinov P. On the constraint function method for contact problems. Computers & Structures 1997;64(5/6):1069–85.
[37] Thorton PM, Mahmood HF, Magee CL. Energy absorption by structural collapse. In: Jones N, Wierzbicki T, editors. Structural crashworthiness. London: Butterworths; 1983. p. 96–117.